2012

Kinetics and reaction chemistryifor slow pyrolysis of enzymatic hydrolysis lignin and organosolv extracted lignin derived from maplewood

George W Huber, *University of Massachusetts - Amherst*
J. Cho
S. Chu
P. J Dauenhaue

Green Chemistry

Cite this: *Green Chem.*, 2012, **14**, 428

www.rsc.org/greenchem

PAPER

Kinetics and reaction chemistry for slow pyrolysis of enzymatic hydrolysis lignin and organosolv extracted lignin derived from maplewood†

Joungmo Cho, Sheng Chu, Paul J. Dauenhauer and George W. Huber*

Received 2nd October 2011, Accepted 10th November 2011
DOI: 10.1039/c1gc16222e

The kinetics and reaction chemistry for the pyrolysis of Maplewood lignin were investigated using both a pyroprobe reactor and a thermogravimetric analyser mass spectrometry (TGA-MS). Lignin residue after enzymatic hydrolysis and organosolv lignin derived from Maplewood were used to measure the kinetic behaviours of lignin pyrolysis and to analyse pyrolysis product distributions. The enzymatic lignin residue pyrolyzed at lower temperature than that of organosolv lignin. The differential thermogravimetric (DTG) peaks for pyrolysis of the enzymatic residue were more similar to the DTG peaks for pyrolysis of the original Maplewood than DTG of the organosolv lignin. The condensable liquid volatile products were collected from a Pyroprobe reactor with a liquid nitrogen trap. The primary monomeric phenolic compounds were guaiacol, syringol, and vanillic acid. However, only 14–36 carbon% of the sample could be detected by GC-MS. Over 60 carbon% of the condensable products were heavy tar molecules that are not detectable by GC-MS. These heavy tar molecules are the primary products from pyrolysis of lignin. Intermediate solid samples were also collected at various pyrolysis temperatures and characterized by elemental analysis, FT-IR, DP-MAS ^{13}C NMR, and TOC. The methoxy groups and ether linkages decreased and the non-protonated aromatic carbon–carbon bonds increased in the solid residues as the pyrolysis temperature increased. The carbon content of the initial lignin feed (derived from enzymatic hydrolysis) and the solid polyaromatics residue (obtained at 773 K) was 58 wt% and 74 wt% respectively. This polyaromatic residue contained about 69 wt% of the original lignin feed. The solid polyaromatics undergo further slow decomposition accompanied by a constant release of carbon dioxide as the pyrolysis reaction continues. The pyrolysis of the enzymatic lignin residue was modelled by two reactions in series. In the first pyrolysis step the lignin was decomposed with an apparent activation energy of 74 kJ mol^{-1} and a heat of reaction of –8,780 kJ kg^{-1}. The second pyrolysis step had an apparent activation energy of 110 kJ mol^{-1} and a heat of reaction of –2,819 kJ kg^{-1}. Lignin pyrolysis has lower activation energies and higher heats of reaction than cellulose pyrolysis.

Introduction

Fast pyrolysis has attracted numerous interest as a viable and promising technique to convert lignocellulosic biomass into valuable chemicals or fuel.[1–8] Lignocellulosic biomass consists of three major components (cellulose, hemicellulose and lignin) that exhibit significantly different decomposition behaviours. Lignin is the second most abundant macrocomponent present in biomass. Industrial lignins are mostly available as byproducts which are commonly used for a heat source to generate process steam.[9] Efficient catalytic upgrading or accurate control of chemical routes that allow the conversion of lignin into liquid transportation fuels have not been developed yet due to the limited understanding and ability to manipulate the underlying reaction chemistry.[10,11] Nevertheless, lignin has gained numerous interest as a feedstock for liquid fuel production due to its aromatic based structure, high energy density and abundance in nature.[11]

Lignin has a complex amorphous structure that mainly consists of methoxylated phenylpropane units connected by various linkages. Formation of lignin is considered to involve polymerization steps of three monolignols: *p*-coumaryl, coniferyl and sinapyl alcohols.[12] Fig. 1 shows the illustrative model structure of lignin and common linkages.[13] Ether linkages

Department of Chemical Engineering, University of Massachusetts, Amherst, 686 North Pleasant Street, 159 Goessmann Lab, Amherst, MA, 01003, USA. E-mail: huber@ecs.umass.edu; Fax: +1 413-545-1647; Tel: +1 413-545-0276

† Electronic supplementary information (ESI) available. See DOI: 10.1039/c1gc16222e

Table 1 Proportion of major linkages in lignin[14]

Linkages	Type	Softwood (%)	Hardwood (%)
β-*O*-4-Aryl ether	C–O–C	46	60
α-*O*-4-Aryl ether	C–O–C	6–8	6–8
4-*O*-5-Diaryl ether	C–O–C	3.5–4	6.5
β-5-Phenylcoumaran	C–C	9–12	6
5-5-Biphenyl	C–C	9.5–11	4.5
β-1-(1,2-Diarylpropane)	C–C	7	7
β-β-(Resinol)	C–C	2	3
Other	—	13	5

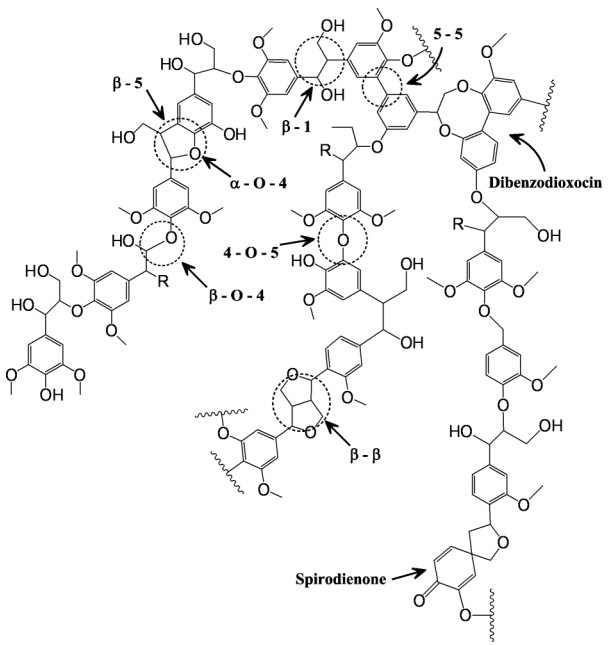

Fig. 1 Illustrative model of enzymatic lignin residue and common linkage types (Adapted from ref. 13, 62, 63).

occupy the largest proportion of lignin regardless of its origin, *i.e.* softwood or hardwood lignin. Among them β-*O*-4 is the most common ether linkage as summarized in Table 1.[14] In addition to the ether linkages, C–C bonds including β-5, 5-5, β-1 and β-β also play a role in connecting lignin monomeric aromatic substructure.

The lignin structures and composition of functional groups widely vary depending on the origin of biomass. It is generally known that the isolation of lignin compounds from original biomass is difficult to achieve without chemical modification.[15] Lignin extractives are mainly classified into two different categories based on the separation methods.[16] One is the lignin extracted by its dissolution in solvent and the other is the lignin residue obtained after removal of sugar components by hydrolysis. In the former method, lignin linkages are broken by strong acid,[17,18] base catalysts[19] or mechanical stress.[20] Resulting smaller fragments of lignin are dissolved in the solvent to be extracted. In the latter method, cellulose and hemicellulose are hydrolyzed by acids[21,22] or enzymes.[23] Resulting sugar monomers are soluble in a liquid mixture and the lignin compound remains as an insoluble solid residue. Thus it is expected that the lignin residue obtained from hydrolysis is more similar to the original lignin than the lignin extracted in a solvent since the lignin residues are exposed to less severe chemical reactions.

The kinetics of cellulose pyrolysis can be understood by the formation of active cellulose followed by reactions that form volatile organic compounds, char, and gases such as carbon dioxide.[24–34] The cellulose kinetics can be modelled by first order reaction models.[33–40] Pyrolysis of lignin occurs over a wider temperature range than that of cellulose.[41] With the increase of temperature, lignin linkages start to break where bond dissociation energy is relatively low. The thermally weak bonds are mainly hydroxyl groups attached to β or γ carbons and ether bonds including β-*O*-4, which are most abundant linkage type in most lignin structures.[14,42] Their bond cleavages contribute to a high production of water and condensable volatile products at low temperature. The methoxyl groups are more resistant against thermal degradation than the ether linkages which allows for the formation of a large fraction of methoxyl phenols such as guaiacol and syringol among condensable volatile products. Thermal decomposition at a low temperature produces a large amount of polyaromatics. Liu *et al.*[43] have observed using GC-MS analysis that lignin pyrolysis at high temperatures (>1000 K) produces fragments of polyaromatics rather than methoxyl phenols in the volatile species.

Understanding the kinetics and chemistry of lignin pyrolysis is critical for the advancement of many different biomass conversion techniques since biomass feedstocks contain a large amount of lignin. A handful of researchers have estimated lumped kinetic parameters of lignin pyrolysis.[16,44–58] Jiang *et al.*[52] summarized the global kinetic parameters from the literature for lignin pyrolysis and estimated by Kissinger's method.[59] The Kissinger method is commonly used to estimate global reaction parameters of biomass pyrolysis by fitting the maximal decomposition temperatures in DTG curves to temperature ramps. They compared kinetic parameters of lignin pyrolysis for four lignin types including alkali lignin, hydrolytic lignin, organosolv lignin, and Klason lignin derived from various hardwoods and softwoods. In general, apparent activation energies for lignin pyrolysis reported in the literature vary from 50 to 150 kJ mol^{-1}. These values are much lower than the activation energy of cellulose pyrolysis (200 kJ mol^{-1}) into volatile organics.[34] When a slow temperature ramp (<10 K min^{-1}) is applied, lignin pyrolysis starts at below 500 K, which is lower than the onset of hemicellulose and cellulose decomposition.[41,53] The lignin pyrolysis however occurs over a very broad temperature range. A wide variety of C–O and C–C linkages are broken during lignin pyrolysis which might be better described by a correlation with the discrepancy of activation energy barriers. Some literature[52,60] employed the distributed activation energy models (DAEM) that fit activation energies by regression with pseudo reaction steps having different reaction orders. However, the DAEM model does not reflect a specific chemical mechanism. Despite the complex reaction chemistry of lignin pyrolysis, the majority of kinetic models have been developed based on the assumption of a first order single step reaction.[16] However, it has been reported that lignin pyrolysis undergoes multiple decomposition steps relying on the pyrolysis temperature.[54,55]

There have been limited efforts to try and identify the temperature dependence of the lignin pyrolysis products.

Iatridis *et al.*[56] conducted the pyrolysis experiments for a precipitated Kraft lignin. They measured the formation of tar, gas, monomeric phenols and the weight change of solid species as a function of temperature and time. They observed that a pyrolysis temperature of 473 K is sufficient to produce volatile species from lignin pyrolysis and the final weight loss increases with temperature (65% weight loss at 1023 K) by producing volatile species. However, they were not able to establish an accurate kinetic model describing the lignin pyrolysis due to the lack of information on the reaction mechanism. Avni[51,57,58] and King[49] studied the pyrolysis of several lignin species extracted by hydrolysis and ethanol organosolv methods from aspen and pinewood. They observed that the major gas species and tar products were CO, CO_2, H_2O, CH_4, SO_2, CS_2, C_2H_2, C_2H_4, C_3H_6, benzene, heavy paraffins and olefins, in their experiments. An *in situ* FT-IR with low resolution spectra was used to determine the production rates of gaseous and volatile species. They claimed that the predicted activation energy for the evolution of volatile chemicals (48 kcal mol^{-1}) is in a very good agreement with the estimated activation energy of the ether linkages connecting the phenyl propane subunits. Nunn *et al.*[55] employed a captive sample electrical screen heater reactor to investigate pyrolysis products changes along reaction temperature. They have performed gas chromatographic analysis for non-condensable gaseous and light condensable product distribution as a function of temperature but not for major phenolic compounds standing for heavy liquid volatile products from lignin pyrolysis. They observed continuous evolution of CO, CO_2 and CH_4 after the cessation of significant weight loss above 1050 K. They stated that this might be due to secondary cracking of tar. Similar results were reported by Caballero *et al.*[44] They employed a pyroprobe reactor to analyze the primary pyrolysis products of Kraft lignin at high temperature ramps. They combined mass and energy balance equations to estimate kinetic parameters. They derived temperature dependences of pre-exponential factor and activation energy which seem not applicable for the general description of intrinsic kinetics. Very recently, Jiang *et al.*[61] reported the temperature effect on the distribution of pyrolysis products from Alcell and Asian lignins using a Py-GC-MS, however the correlation with kinetic model was not established.

The objective of this study is to develop a lumped kinetic model of lignin pyrolysis at low temperatures (<673 K) that utilizes mechanistic insight derived from chemical analysis of lignin chemistry. We have tested two different lignin types extracted from Maplewood (lignin residue after enzymatic hydrolysis and organosolv lignin) for the kinetic study of lignin pyrolysis. The pyrolysis of each lignin sample was conducted in both a TGA and a pyroprobe reactor, and compared with the original Maplewood sample. One plausible lumped reaction mechanism was proposed, and the governing rate equations were derived. Constant temperature and dynamic experimental data from thermogravimetric analysis were used to compare with the kinetic model to estimate rate parameters correlated by the Arrhenius equation. We expect that the kinetic models of different macrocomponents, including lignin in this study, can be further applied to develop an optimal design for biomass conversion technologies which involve pyrolysis of lignin.

Experimental

Materials

In this study, two different types of lignin were prepared to study the reaction chemistry of Maplewood lignin. One sample is lignin residue remaining after enzymatic hydrolysis and the other is ethanol organosolv lignin (hereafter they will be designated by 'solid lignin residue' and 'organosolv lignin' for brevity).

The solid lignin residue was prepared by removal of hemicellulose and cellulose compounds by hydrolysis of Maplewood. The hemicellulose compounds were removed by a hot water pretreatment in a pressurized Parr reactor (620–1517 kPa; 1 L volume) followed by overnight pre-soaking of 10 wt% of Maplewood in water. Filtration and washing produced a solid fraction that mainly contained cellulose and lignin. The pretreated solid was then hydrolysed by enzymes (Spezyme and Novozyme) to remove the cellulose at pH 4.8 and 50 °C to obtain the solid Maplewood lignin residue. The detailed procedures for enzymatic hydrolysis and the composition analysis are described by Jae *et al.*[23] The major impurities in the lignin residue sample were cellulose (11.6 wt%) and hemicellulose (3.3 wt%).

Organosolv lignin was prepared according to the method of Pan *et al.*[17] Maplewood was reacted with ethanol and water mixture (1 : 1) in the presence of 1.25% of sulfuric acid at the temperature of 180 °C for one hour. The resulting liquid mixture was diluted with water to precipitate organosolv lignin. Finally, a solid organosolv lignin sample was prepared by filtration and drying in the oven at 110 °C overnight.

The molecular weights of the samples were measured by gel permeation chromatography (GPC). Shimadzu HPLC system with an UV detector (frequency 254 nm) and Varian Meso-Pore column (part No. 1113–6325) was used with stabilized tetrahydrofuran (THF) as a mobile phase flowing at 0.5 cm^3 min^{-1}. Lignin samples for GPC were prepared by dissolving in THF at 1 wt% concentration. Only 16 wt% of solid lignin residue was dissolved in THF. The solid lignin residue sample did not dissolve completely in THF. We were not able to measure molecular distribution for the insoluble part of solid lignin residue. This insoluble lignin most likely has a higher molecular weight distribution than the soluble fraction.[64] The lignin solutions in THF were filtered with 0.45 μm filter and used for GPC analysis. The GPC column was calibrated with polystyrene molecular weight standards in the range of 162 to 38 640 Da. The resulting GPC diagrams are shown in Fig. 2. The molecular weights of lignin samples are widely distributed between 100 to 10 000 Da. The lignin residue sample shows several peaks having different molecular weights while the organosolv lignin has only one broad peak.

Fourier-transform infrared (FT-IR)

FT-IR spectra for different solid products from lignin pyrolysis were obtained using a Bruker Equinox 55 infrared spectrometer with DRIFTS cell (Praying Mantis™ from Harrick Scientific). The number of scans was set at 100 with a resolution of 4 cm^{-1}, over the range 4000–400 cm^{-1}. Dry powder samples were used directly without dilution in KBr. KBr was used to obtain a background spectrum prior to sample measurements.

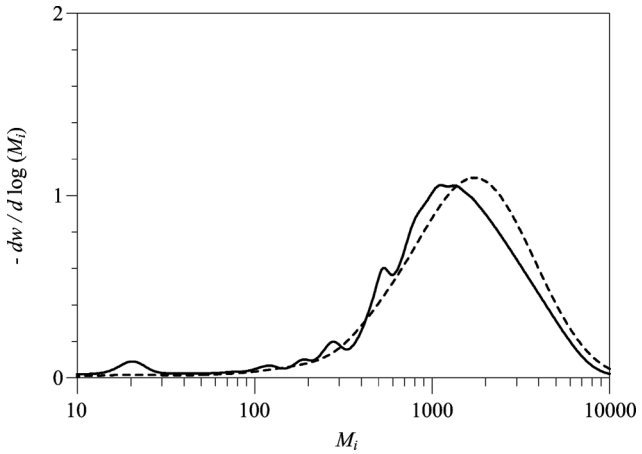

Fig. 2 Molecular weight distribution curves for two types of lignins; (a) solid lignin residue after enzymatic hydrolysis of Maplewood (solid line); (b) lignin from Maplewood by using ethanol/water solution organosolv extraction method (dotted line).

Thermogravimetric analysis (TGA) and differential scanning calorimetry (DSC) analysis

The pyrolysis of lignin was performed in a TGA-DSC (TA instruments SDT Q600 system) to measure the weight loss under dynamic or isothermal conditions. A helium gas (ultra-high-purity grade; 100 ml min^{-1}) was used as a carrier gas sweeping volatile and gas products out of furnace continuously. Different weight loadings (5–25 mg of sample) were used to check the effect of initial sample size of TGA-MS experiment. All samples sizes in the range showed almost identical pyrolysis characteristics. A typical amount of biomass used for the other experiments in the TGA was about 10 mg. Each sample was pre-dried in the TGA at 110 °C for one hour. Gaseous products leaving the TGA were analyzed by a quadrupole mass spectrometry (Extorr XT 300 with an electron ionization voltage at 27 eV). SDT Q600 system was also used to collect intermediate solid samples during the pyrolysis. The sample was heated up to the predetermined final temperature at a temperature ramp of 150 K min^{-1} and a fast He-cooling system to stop the pyrolysis as soon as it reached the reaction temperature. The weight difference right before and after the cooling step was measured to confirm any further decomposition. A negligible amount of weight loss (less than 3 wt%) was detected at this step. The intermediate solid products were recovered and stored in a closed ampoule for further analysis. In addition to TGA, a DSC was used to quantify the heat of reaction for each step.

Pyroprobe reactor with GC-MS and nitrogen trap

Lignin pyrolysis experiments were conducted using a model 2000 pyroprobe analytical pyrolizer (CDS Analytical Inc.). The pyroprobe was connected to a model 5890 gas chromatograph (GC) interfaced with a Hewlett Packard model 5972A mass spectrometer (MS) to quantify the volatile products. A capillary column (Restek Rtx-5sil MS) was used as a stationary phase and a helium gas was used for an inert pyrolysis gas as well as a mobile phase for the GC analysis. Pyroprobe experiments were also conducted in a 20 ml glass vial which was soaked in a liquid nitrogen trap to collect the liquid samples. The same heating ramps applied in the TGA-DSC experiments were applied to most pyrolysis experiments.

DP-MAS ^{13}C NMR

Direct polarization-magic angle spinning was used in this work to analyse intermediate solid product samples obtained from TGA. Samples were packed in a 4-mm-diam zirconia rotor with a Kel-F cap and examined at a ^{13}C frequency of 75.47 MHz in a Bruker DSX-300 spectrometer at a spinning speed of 9 KHz for 24 h. The ^{13}C 180° pulse length was 8 μs and 90° pulse was 4 μs. The decoupling strength of DP-MAS was 60 kHz.

Total organic carbon (TOC)

The carbon content in solid samples was analysed in a total organic carbon analyser. The solid samples were completely combusted at 900 °C under constant oxygen flow in Shimadzu Solid Sample Module SSM-5000A. The amount of carbon dioxide was quantified with Shimadzu TOC-V CPH.

Gel permeation chromatography (GPC)

The samples were dissolved in THF and injected into a Shimadzu HPLC system (SIL-20ACHT Auto sampler, LC-20AD Solvent Delivery Module, DGU-20A5 Degasser, CTO-20A Column Oven, SPD-M20A UV-Vis detector) with Agilent Mesopore column. The molecular weight was calculated based on the series of polystyrene standards. The flow rate of solvent was 0.5 ml min^{-1} and the signal from UV-Vis detector was taken at 254 nm.

Kinetic modelling

TGA has widely been used to develop lumped kinetic models of biomass pyrolysis. Two different approaches are generally employed to study kinetics of biomass pyrolysis: (1) constant temperature experiments and (2) dynamic experiments. Under constant temperature conditions the overall weight loss is measured with time during pyrolysis.

In the current study, we propose that the pyrolysis of lignin follows a two-step reaction pathway. In the first step, lignin decomposes into solid polyaromatics and volatile organic compounds. Volatile products diluted in a carrier gas leave the system. Polyaromatics remain as solids and undergo further decomposition into gas and vapour products in the second step. The governing rate equations are shown in eqn (1) and (2).

$$\frac{dm_L}{dt} = -k_1 m_L \quad (1)$$

$$\frac{dm_P}{dt} = f_P k_1 m_L - k_2 m_P \quad (2)$$

In eqn (1) and (2) k_i is the rate constant at the step i correlated by Arrhenius equation, m_L and m_P are the weight for lignin and polyaromatics in a solid mixture. f_P is the weight fraction for the formation of polyaromatics in the first step. The weight of total solid derived from lignin pyrolysis, η_C, is the sum of lignin and polyaromatics.

$$\eta_L = m_L + m_P \quad (3)$$

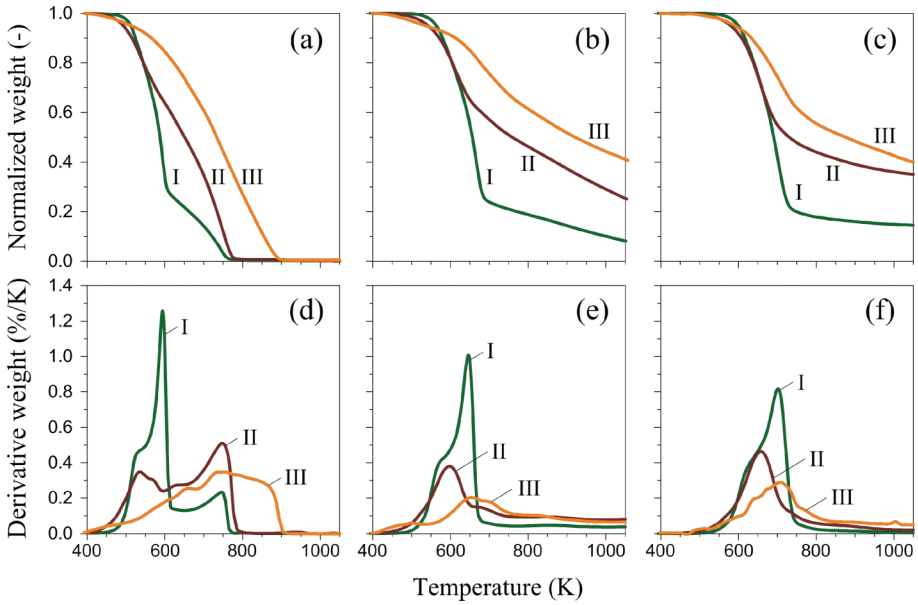

Fig. 3 Thermogravimetric (a, b and c) and differential thermal (d, e, and f) curves for the pyrolysis of Maplewood (I), solid lignin residue after enzymatic hydrolysis (II) and lignin extracted from Maplewood by organosolv method (III) at heating ramps of 1 (a and d) 15 (b and e) and 150 K min^{-1}(c and f).

Solid lignin residue samples contain carbohydrate impurities, which mainly belong to the cellulose fraction in the original biomass. A kinetic model for cellulose was applied to estimate the weight changes of cellulose fraction and overall weight change of the pyrolysis of lignin residue was calculated based on the summation rule.[65] The overall weight observed in TGA for the pyrolysis of lignin residue is shown in eqn (4).

$$\eta = \alpha_L \eta_L + \alpha_C \eta_C \quad (4)$$

In eqn (4) η_C is the weight of solid derived by cellulose pyrolysis. α_L and α_C are the fractions of lignin and cellulose in lignin residue sample, respectively.

The kinetic parameters for lignin pyrolysis were obtained by adjusting the model parameters to all experimental data. During parameter estimation, the objective function given in eqn (5) was minimized.

$$\text{error sum} = \sum_i \sum_j \left| \eta_{ij}^{\text{exp}} - \eta_{ij}^{\text{calc}} \right| \quad (5)$$

In eqn (5) i and j denote the index for recorded experimental data points in the TGA and the index for data set in isothermal or dynamic experiments, respectively. The model was prepared using a Matlab code, 'ode23.m' was used to solve coupled ordinary differential equations.

Results and discussion

Pyrolysis of biomass samples in TGA

The pyrolysis behaviours of raw Maplewood, solid lignin residue, and organosolv lignin were measured by TGA as shown in Fig. 3. A significant weight loss by multiple decompositions was observed at a temperature range between 400–1000 K. With the slow temperature ramp of 1 K min^{-1}, decomposition of both Maplewood and solid lignin residue are completed at about 775 K. However, organosolv lignin exhibits decomposition at a higher temperature and completely disappears at 900 K. During lignin pyrolysis, more than 25% of initial weight was volatilized at a low temperature (<700 K) and a slow weight loss was observed at a higher temperature. Only a small fraction (20–30%) of raw Maplewood is converted into the solid intermediate products. The lignin samples produce more solid intermediate products at the faster temperature ramp. The organosolv lignin produced more solid intermediate products than the solid lignin residue.

A DTG curve for biomass pyrolysis gives another insight into the pyrolysis of each macrocomponent. Hemicellulose and cellulose decompose at 495–590 K and at 590–673 K at 10 K min^{-1}, respectively.[41,65] Lignin decomposes at a broad temperature range from 400 to 1273 K, which varies depending on the lignin type.[16,41] The first decomposition peak for Maplewood pyrolysis at 1 K min^{-1} appears around 525 K, and a narrow peak appears at 590 K. These first two peaks correspond to the decomposition of hemicellulose and cellulose, respectively.[23,33] With an increase of temperature, the decomposition continues until it reaches 775 K. The corresponding DTG curve (at 600–775 K) is broad compared to peaks of hemicellulose and cellulose. The maximum decomposition rate occurs at 740–750 K. This matches with solid lignin residue and ethanol organosolv lignin. The DTG curve for organosolv lignin shows a wider decomposition pattern at a higher temperature than the solid lignin residue. This implies that solid lignin residue is more representative than organosolv lignin to study the kinetics of lignin in virgin biomass.

Preparation of solid intermediate product

The pyrolysis of lignin results in a weight loss of sample by releasing volatile products and accumulating a highly carbonized material in a residual solid mixture which we will refer to as

Table 2 Elemental analysis for original Maplewood lignins and solid product samples obtained at (a) 373, (b) 648, (c) 713, and (d) 773 K during the pyrolysis of lignin residue from enzymatic hydrolysis at a heating ramp of 150 K min^{-1}

Sample	C (wt%)	H (wt%)	O (wt%)	H/C_{eff}[a]
Organosolv lignin	64.94	5.39	29.67	0.31
Maplewood	48.59	5.92	45.49	0.06
a[b]	58.81	5.70	35.49	0.26
b	66.37	4.89	28.74	0.23
c	72.20	4.12	23.68	0.19
d	74.25	3.60	22.15	0.13

[a] $H/C_{eff} = (H - 2O)/C$ where H, C, and O are molar number of hydrogen, carbon, and oxygen atoms, respectively. [b] Predried sample for solid lignin residue.

'polyaromatics' in this paper. The polyaromatics yield from cellulose increases with decreasing temperature or decreasing temperature ramps.[34,66] In contrast, the polyaromatics yield from lignin pyrolysis increases with temperature ramp as shown in Fig. 3. We employed a TGA to collect three intermediate solid product samples of the solid lignin residue as a function of time at a temperature ramp of 150 K min^{-1} as shown in Fig. 4. Elemental analysis of each sample is summarized in Table 2. The weight percent of carbon in the samples increased with increasing temperature. The weight fraction of oxygen and hydrogen in the samples decreased with increasing temperature.

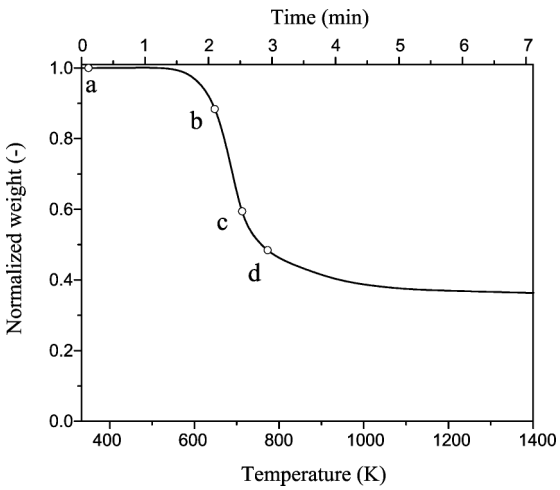

Fig. 4 Thermogravimetric curve for the pyrolysis of Maplewood lignin residue from enzymatic hydrolysis at a heating ramp of 150 K min^{-1}. Circles are the points where solid samples are taken for analysis.

More than 40 wt% of lignin residue can be volatilized in the first decomposition step (shown as point C in Fig. 4). As a result, a significant amount of carbon is concentrated in a solid mixture. Several phenolic compounds are detected as condensable liquid products and their analysis is discussed in later sections. Carbon monoxide, carbon dioxide and water were the major gases species identified by the MS connected to TGA *via* a heated line minimizing condensation of light molecules.

The effective hydrogen-to-carbon ratio (H/C_{eff}) is a measure of the effective amount of hydrogen in a biomass feedstock.[67,68] Most biomass feedstocks have H/C_{eff} ratios lower than 0.5 due to high oxygen contents while petroleum-based feedstocks have a value between 1–2.[69] The Maplewood has a low value, 0.06 due to high oxygen content. The organosolv lignin has H/C_{eff} ratio five times that of original Maplewood. This implies that lignin compounds have a high relative hydrogen content compared to the cellulose and hemicellulose fraction of the biomass. The H/C_{eff} ratio in the solid lignin residues decreases with increasing pyrolysis temperature.

Analysis of lignin pyrolysis products

The IR spectra of solid lignin residue and its intermediate solid pyrolysis products were measured at room temperature to examine how the functional groups of the solid residue change with temperature as shown in Fig. 5. The characteristic wavelengths of various functional groups are listed in Table 3. There are two characteristic wavenumber regions (2800–3500 cm^{-1} and 600–1750 cm^{-1}) that are indicative of the structure of lignin and the thermal degradation due to pyrolysis.

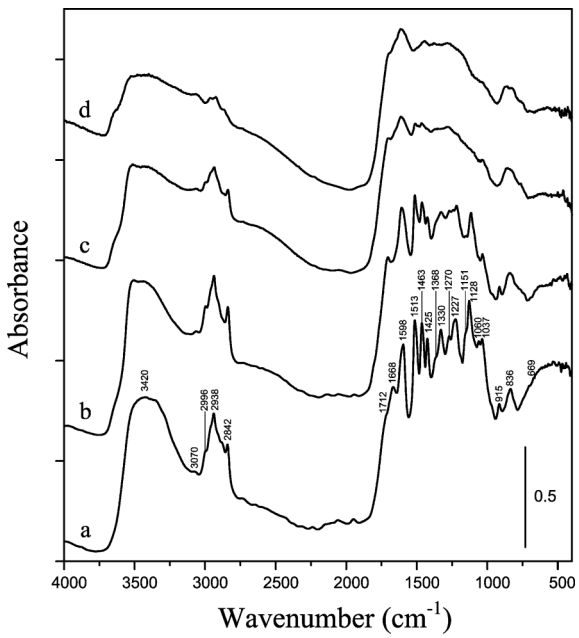

Fig. 5 FT-IR spectra of (a) solid lignin residue from enzymatic hydrolysis, and solid product samples obtained at (b) 648 K, (c) 713 K, and (d) 773 K during the pyrolysis at a heating ramp of 150 K min^{-1}.

The broad band at 3420 cm^{-1} (OH stretching vibration) decreases with increasing pyrolysis temperature. The OH stretching

Table 3 Characterization of FT-IR spectra of solid lignin residue from enzymatic hydrolysis and solid product samples by pyrolysis

Band (cm^{-1})	Characteristics	Changes	Ref.
3420	OH stretching	Decrease	70,71
3070	Aromatic CH stretching	Increase	71
2938	Aliphatic CH stretching	Decrease	71
2842	Methoxyl	Disappear	71
1712, 1668	C=O stretching (aromatic ring)	Decrease	70
1598, 1513,1425	Aromatic ring vibration	Decrease	70,71
1463,1368	CH deformation	Decrease	70
1330	Syringyl	Disappear	70
1270	Guaiacyl	Decrease	70
1060,1037	CH & CO deformation	Decrease	70
915,836	Aryl CH wags	Persist	71
669	OH out of plane bending	Disappear	71

vibration is due to phenolic groups and adsorbed water. The bands at 3070 and 2938 cm^{-1} indicate aromatic and aliphatic CH stretching respectively. It is notable that the band at 3070 cm^{-1} indicating aromatic CH stretching increases with pyrolysis temperature while the band at 2938 cm^{-1} decreases. This implies that the carbon from lignin pyrolysis is accumulated in the form of polyaromatic rings. There was a clear disappearance of the band at 2842 cm^{-1} indicating methoxyl group decrease with increasing temperature.

A carbonyl group characterized by bands at 1712 and 1668 cm^{-1} decreases with increasing temperature. The syringyl and guaiacyl group bands appear at 1330 and 1270 cm^{-1}, respectively. These two are characteristic bands for lignin compounds. Similar to a previous IR spectral study of lignin pyrolysis,[70] it was observed that the predominant intensities of syringyl and guaiacyl groups disappear first with an increase of pyrolysis temperature. This indicates that the mechanism of lignin pyrolysis initially includes the loss of ether linkages.

DP-MAS results and the chemical shifts of the major peaks of the solid pyrolysis samples are shown in Fig. 6 and Table 4. Peak 1 belongs to methoxy groups. This peak disappears as the temperature increases. Peak 2 is an overlap of the Cα-OR in lignin and CHOH of carbohydrates. We can also see a cellulose peak at 104 PPM (labelled peak 3). This peak decreases at 648 K, which is the temperature where most cellulose decomposes.[33] The Cα-OR peak, which corresponds to α ether bond, disappears with increasing temperature. The β-*O*-4 linkage is in the range of 82–86 ppm. This peak disappears at a temperature of 648 K. Peak 3 in the 98–142 ppm is the non-protonated aromatic C–C and some carbohydrate peaks. A broad peak, at 98–142 ppm, with an aromatic chemical shift forms at 773 K. The solid left

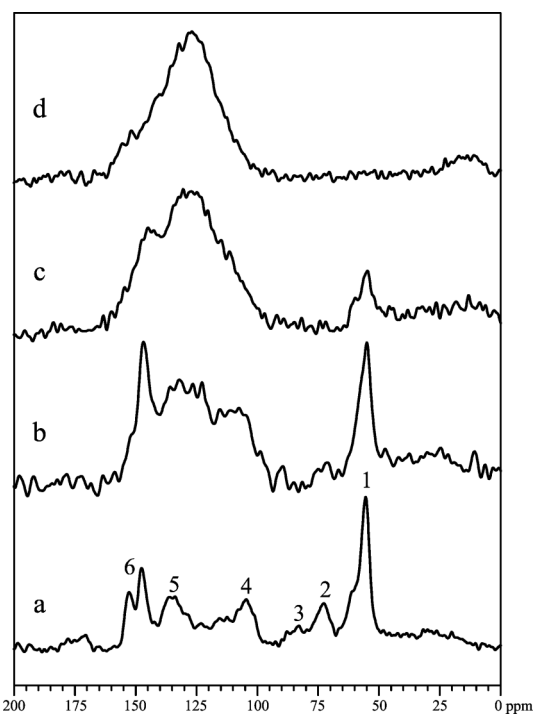

Fig. 6 Direct polarization/magic angle spinning (DP/MAS) spectra of (a) solid lignin residue from enzymatic hydrolysis, and solid product samples obtained at (b) 648, (c) 713, and (d) 773 K during the pyrolysis at a heating ramp of 150 K min^{-1}.

Table 4 NMR chemical shifts[63] of solid lignin residue from enzymatic hydrolysis

Peak number	Chemical shift (ppm)	Moiety
1	56	Methoxy group
2	73	C_α-OR of lignin and CHOH of carbohydrates
3	82–86	C_β-OR of lignin
4	104	OCHO of carbohydrates
5	135	Aromatic carbon
6	147,152	Aromatic C–O

Table 5 Percentage of total spectral area assigned to methoxy group and nonprotonated aromatic carbon from DP/MAS for (a) solid lignin residue from enzymatic hydrolysis, and solid product samples obtained at (b) 648, (c) 713, and (d) 773 K during the pyrolysis at a heating ramp of 150 K min^{-1}

Sample	48–61.2 ppm (Methoxy group)	98–142 ppm (Nonprotonated aromatic C–C)
a	21.95%	31.4%
b	16.95%	43.34%
c	7.17%	52.68%
d	2.3%	61.64%

after the lignin pyrolysis has an aromatic-based structure consisting primarily of non-protonated aromatic C–C bonds. Table 5 summarizes the quantitative analysis of lignin characteristic peaks during pyrolysis. The fraction of spectral area for methoxy group decreases from 21.95 to 2.3% as temperature increases while that of the non-protonated aromatic C–C increases from 31.4 to 61.64%. These results imply that the intermediate solid products obtained from lignin pyrolysis are mainly composed of polyaromatics. These results are consistent with the work of Sharma *et al.*[71] Wang and Low[72] claimed that small reactive fragments (alkene-like compounds) and monomeric aromatic rings evolve at a lower temperature and form nuclei which could be a precursor of cyclic polycarbon structure. At a higher temperature, these units are further polymerized to form larger polyaromatics. Other researchers[42,73,74] have concluded that homolytic bond cleavages, such as O-CH_3 and ether bonds, cause radical formation, which subsequently forms polycyclic aromatic ring.

The lignin samples were pyrolyzed in a pyroprobe GC-MS system under three temperatures at a temperature ramp of 150 K min^{-1}. Table 6 lists the products from pyrolysis of these samples. Between 68 to 93 wt% of the products produced by pyrolysis in the pyroprobe reactor were solids. In general, the pyrolysis of biomass in the pyroprobe produces more char than the pyrolysis in a TGA system. This is because a high concentration of pyrolysis vapors form in the pyroprobe which induces further repolymerization or condensation, followed by secondary reaction steps forming gas and coke.[23,33] Between 0.2 to 6.7 wt% of the products were gases. The detected components in the gas include carbon monoxide, carbon dioxide and water. Liquid products were collected by conducting the experiments in a 20 ml vial that was in a He atmosphere, which was soaked in the liquid nitrogen to condense vapour products. In each experiment, 6 to 24 wt% of liquid products can be collected. A lower amount of liquid and gaseous products were produced

Table 6 Overall weight distribution (wt%) of pyrolysis products of solid lignin residue from enzymatic hydrolysis and ethanol organosolv lignin from a pyroprobe reactor. Vapor and solid samples were collected using a pyroprobe reactor with nitrogen trap at a heating ramp of 150 K min^{-1}

	Solid lignin residue			Ethanol organosolv lignin		
T/K	Gas[a]	Liquid	Solid	Gas[a]	Liquid	Solid
648	1.58	6.11	92.31	0.21	6.49	93.3
713	4.37	8.15	87.48	1.46	8.24	90.3
773	6.73	24.42	68.85	3.09	16.01	80.9

[a] Estimated based on mass balance.

from the ethanol organosolv lignin compared to the solid lignin residue.

Table 7 shows the carbon balance for pyrolysis of the lignin samples in the pyroprobe reactor. The solid products (unreacted lignin and solid polyaromatic products) contained most of the carbon (64–87%). The gaseous products contained less than 6% of the carbon. Gaseous products mainly contain carbon monoxide and carbon dioxide. Ethanol organosolv lignin had much less gas production than solid lignin residue at the same pyrolysis conditions. 12 to 30% of carbon was collected as liquid condensate.

Table 8 shows the carbon selectivity of each quantifiable product in the liquid samples which are analysed by GC-MS. Carbon selectivity is defined by carbon content in each species divided by the overall carbon amount in the detectable liquid and unidentified products. We were only able to quantify 14 to 36 carbon% of the products in the liquid product with most of these products being monomeric aromatics. Guaiacol, syringol and vanillic acid are the highest observable detectable compounds even though each of these compounds has a carbon selectivity of less than 6.0%. These results agree with the recent analysis of volatile products from lignin pyrolysis reported by Bridgwater *et al.*[61] They mentioned that unidentifiable products in their analysis are most likely larger molecular weight compounds that are formed from lignin pyrolysis while monomeric products come from the ether bond cleavages in lignin. The ether bond is easy to break due to low dissociation energy.[75] Kawamoto *et al.*[76] proposed the reaction mechanism that the bond cleavages during lignin pyrolysis results from radical reactions including

Table 7 Carbon balance (carbon molar%) of pyrolysis products of solid lignin residue from enzymatic hydrolysis and ethanol organosolv lignin obtained from Py-GC-MS analysis with a heating ramp of 150 K min^{-1}

T/K	Gas[a]	Liquid[b]	Solid	Unidentified[c]
Solid lignin residue				
648	0.46	1.73	87.43	10.38
713	5.39	2.67	80.59	11.35
773	6.00	10.68	64.34	18.98
Ethanol organosolv lignin				
648	0.04	0.38	87.18	12.40
713	0.36	1.01	82.90	15.73
773	0.75	4.00	81.94	13.31

[a] Gases are a mixture of CO and CO_2. [b] Products detected from GC-MS. [c] Heavy liquid condensates which can't be detected in GC-MS; carbons are estimated based on the balance.

H-abstraction on phenolic group. They claimed that C_β–O bond homolysis generating radical species initiates chain reactions.

Fig. 7 shows a weight loss curve of lignin residue from TGA measurement and corresponding mass spectra of gaseous species as a function of time. Isothermal conditions were kept at 1273 K, after a temperature increase from 323 K to 1237 K with a temperature ramp of 50 K min^{-1}, to observe gas-phase changes during decomposition. Within 10 min, 60% of the initial product weight was volatilized with the remaining mass pyrolyzing after about 40 min. The volatile species were mainly water, carbon dioxide and carbon monoxide in the first decomposition step as shown in Fig. 7. Small peaks of CH_4 and H_2 were also detected. This implies that the lignin pyrolysis accompanies minor dehydrogenation and demethanation in the first decomposition step. The CO_2 concentration did not change through the overall decomposition. No detectable other gases were found after the initial decomposition step. This suggests that the residual carbon may undergo oxidation by the low levels of oxygen forming CO_2 at the higher temperatures.

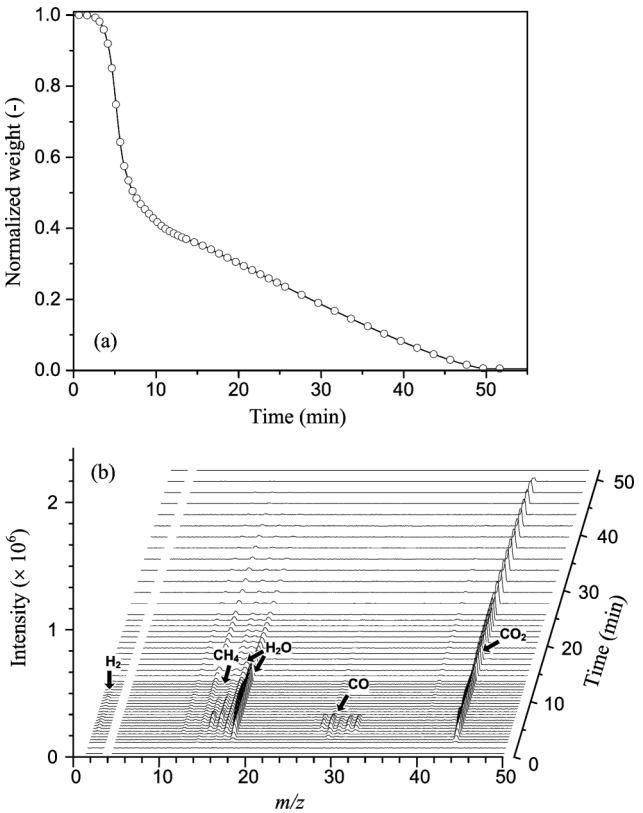

Fig. 7 (a) TGA curve for lignin pyrolysis and (b) mass spectrum for gaseous products leaving TGA as a function of time. A constant temperature ramp of 50 K min^{-1} followed by an isothermal condition at 1273 K was applied to the cold lignin sample (323 K) for the pyrolysis.

Reaction pathway for lignin pyrolysis

Fig. 8 shows our proposed lumped reaction mechanism of lignin pyrolysis based on experimental observation. The molecular formula of Maplewood lignin was estimated from the average molecular weight measured by GPC and from elemental analysis of lignin residue. Maplewood lignin undergoes a fast

Table 8 Carbon selectivity (%) of condensed liquid products from a Py-GC-MS analysis for solid lignin residue after enzymatic hydrolysis at a heating ramp of 150 K min^{-1}

Product	Formula	Solid lignin residue			Ethanol organosolv lignin		
		648 K	713 K	773 K	648 K	713 K	773 K
Furfural	$C_5H_4O_2$	0.00	0.00	0.00	0.00	0.01	1.59
5-Methylfurfural	$C_6H_6O_2$	0.00	0.00	0.00	0.02	0.01	0.10
Furfural alcohol	$C_5H_6O_2$	0.60	2.34	1.61	0.00	0.00	0.00
Phenol	C_6H_6O	0.00	0.00	0.33	0.00	0.00	0.13
3-Methyl-1,2-cyclopentanedione	$C_6H_8O_2$	0.00	0.00	0.00	0.02	0.02	0.22
4-methylphenol	$C_7H_8O_1$	0.00	0.00	0.00	0.00	0.00	0.07
Guaiacol	$C_7H_8O_2$	0.06	0.18	3.02	0.04	0.08	0.93
Benzoic acid	$C_7H_6O_2$	0.13	0.10	0.13	0.05	0.10	0.44
2-Methoxy-4-methylphenol	$C_8H_{10}O_2$	0.21	0.01	1.24	0.12	0.36	1.95
2,3-Dimethoxy toluene	$C_9H_{12}O_2$	0.08	0.02	1.06	0.00	0.00	0.00
3-Methoxy-1,2-benzenediol	$C_7H_8O_3$	0.36	0.04	2.13	0.00	0.06	0.80
4-Ethyl-2-methoxyphenol	$C_9H_{12}O_2$	0.00	0.00	0.00	0.06	0.05	0.70
4-Methylcatechol	$C_7H_8O_2$	0.00	0.00	0.00	0.05	0.09	0.26
4-Hydroxy-3-methylacetophenone	$C_9H_{10}O_2$	0.26	0.20	1.55	0.07	0.03	0.41
Syringol	$C_8H_{10}O_3$	2.53	2.51	5.76	0.03	0.24	2.67
Vanillin	$C_8H_8O_3$	1.55	1.18	1.68	0.05	0.18	1.19
Vanillic acid	$C_8H_8O_4$	2.81	2.00	5.10	0.16	0.61	3.97
1-[4-Hydroxy-3-methoxyphenyl]-ethanone	$C_9H_{10}O_3$	0.30	0.42	0.90	0.65	0.96	3.27
1,2,3-trimethoxy-5-methyl-benzene	$C_{10}H_{14}O_3$	1.94	1.20	3.60	0.04	0.47	1.41
4-Methyl-2,5-dimethoxybenzaldehyde	$C_{10}H_{12}O_3$	0.45	0.27	1.27	0.22	0.06	1.66
Diethyl phthalate	$C_{12}H_{14}O_4$	0.55	2.38	1.18	0.00	0.00	0.00
4-Hydroxy-3,5-dimethoxybenzaldehyde	$C_9H_{10}O_4$	1.01	1.75	1.54	0.59	0.08	0.21
Phenol, 2,6-dimethoxy-4-[2-propenyl]-	$C_{11}H_{14}O_3$	0.85	2.04	1.96	0.68	0.17	0.23
1-[4-Hydroxy-3,5-dimethoxyphenyl]ethanone	$C_{10}H_{12}O_4$	0.04	0.64	0.54	0.06	0.16	0.01
1-[2,4,6-Trihydroxy-3-methyl]-1-butanone	$C_{10}H_{12}O_4$	0.46	1.62	1.34	1.10	0.10	0.83
Unidentified		85.81	81.1	64.06	95.99	96.16	76.95

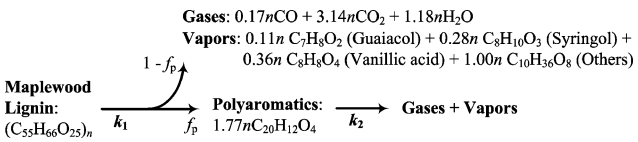

Fig. 8 Proposed reaction pathway of lignin pyrolysis.

decomposition at a low temperature and produces solid polyaromatic hydrocarbons and volatile products. Overall material and carbon balance equations were used to calculate the stochiometric coefficients in the proposed reaction pathways. The major volatile species include gaseous products (mainly water, carbon dioxide and carbon monoxide) as well as condensable liquid products (*e.g.* guaiacol, syringol and vanillic acid). The vapour composition was calculated based on the detectable products accumulated after the pyrolysis of lignin residue from ambient up to 773 K. The weight fraction converted into volatile species ($1 - f_p$) was about 0.31. This value coincides with the estimated value obtained from the lumped kinetic model fit to dynamic experimental data in TGA which will be discussed later. The molecular formula of solid polyaromatic products was calculated based on the work of Sharma[71] and the carbon balance of lignin residue pyrolysis at 773 K.

Kinetic parameters and heats of reaction for lignin pyrolysis

Few kinetic studies have been made for lignin pyrolysis compared to cellulose pyrolysis. Past kinetic parameter estimations were mainly done by comparing the global decomposition models with the observed weight loss. Nunn *et al.*[55] estimated that the activation energy for milled wood lignin from sweet gum is 82.0 kJ mol^{-1} from fitting the global decomposition rate. Várhegyi *et al.*[53] reported relatively small activation energies of 34–65 kJ mol^{-1} for various milled wood lignins. Liu *et al.*[54] developed a reaction model based on the two-step reaction pathway similar to the one proposed by current study (Fig. 8). They estimated that activation energies for the pyrolysis of Fir lignin are 72.9 (E_1), 136.9 kJ mol^{-1} (E_2) and those of Birch lignin 87.2 (E_1), 141.7 kJ mol^{-1} (E_2), respectively. More recently, Jiang *et al.*[16] have reported rate parameters for the pyrolysis of various lignin types. In their model, the reaction order was assumed not to be one and was estimated as an adjustable parameter. They estimated the reaction orders for most lignin to be one except for Klason lignin ($n \sim 1.5$). The estimated activation energies (134–172 kJ mol^{-1}) were higher than those values in other lignin pyrolysis studies.[44–52,54,55]

In our work, TGA experiments were performed under both dynamic and constant temperature conditions to measure the kinetic behaviour of lignin pyrolysis. The pyrolysis of solid lignin residue was carried out at various temperature ramps for the dynamic measurements (see Fig. S1 in supplementary information†). The temperature at which decomposition initiates in lignin pyrolysis increased with increasing temperature ramp. In general, when a faster temperature ramp is applied to biomass pyrolysis in a TGA experiment, a greater delay in thermal decomposition is observed. The thermal delay is ascribed to the non-isothermal temperature distribution between lignin sample and external measurement.[77] Such thermal delay appearing in dynamic TGA experiments can be accounted for to estimate kinetic parameters by incorporating the characteristic rate equations into the thermal-lag models. Thermal-lag models are developed based on the energy balance across the sample

boundary and simplify the description of heat transfer within the TGA to a single coefficient.[33] We estimated kinetic parameters by utilizing a thermal-lag correction factor to account for non-isothermal reaction conditions. The first decomposition was fit to the activation energy of 74.1 kJ mol^{-1} using the thermal-lag model and the weight fraction of polyaromatics of 0.69. The observed and estimated weight changes for different temperature ramps are shown in Fig. 9. Antal[78] reported similar values (0.65) for the fraction of solid intermediate with the pyrolysis of Kraft Pine lignin. He assumed that volatile products from pyrolysis of lignin subsequently follow the competing decomposition pathways in a similar way to the pyrolysis of cellulose with activation energy differences of 54.8 kJ mol^{-1} between gas and condensable liquid product formation. The decomposition of solid polyaromatics occurs over the wider temperature range and is significantly delayed by a fast temperature ramp. We were not able to develop any relevant thermal-lag models for the secondary decomposition at a fast temperature ramp due to inconsistent thermal decomposition behaviours. In order to develop a reliable reaction-transport model, it is required to combine more detailed information on thermophysical properties of chemical species involved in the reaction.

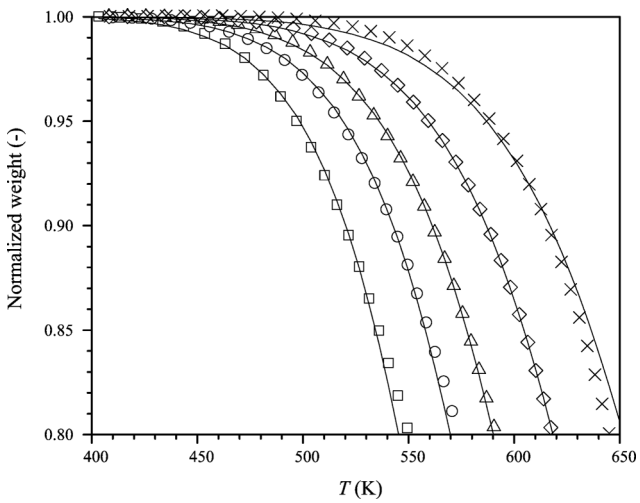

Fig. 9 TGA curves for the initial pyrolysis of solid lignin residue at heating ramps of 1(□), 5(○), 15(△), 50(◇), and 150(×) K min^{-1}. Lines are model estimations for initial decomposition.

The constant temperature TGA experiments were repeated at the temperature range of 523–673 K to evaluate kinetic parameters for both reaction steps of lignin pyrolysis. The kinetic model described by eqn 1–4 was used to fit the constant temperature TGA data. Our kinetic model effectively describes decomposition behaviour during lignin pyrolysis. The resulting model fit and experimental weight changes of constant temperature lignin pyrolysis are shown in Fig. 10. During the parameter estimation, the activation energy estimated from dynamic experiments, E_1, was fixed to reduce the degrees of freedom. The low activation energy barrier for reaction 1 gives rise to the weight loss by volatile species production. At low temperature (523 K), slow decomposition starts after about 20% volatilization. Below this temperature, it is expected that

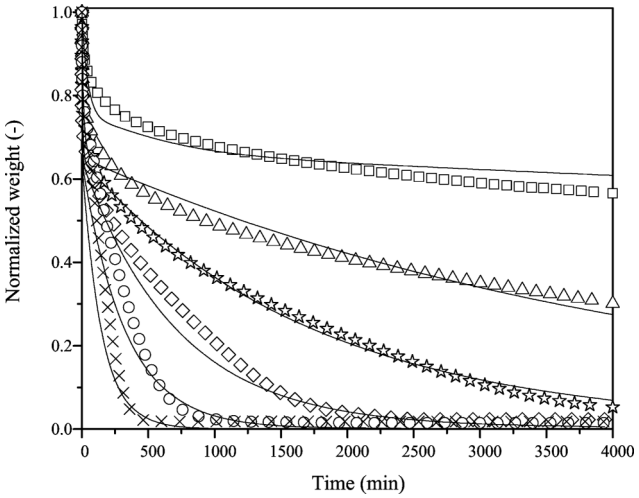

Fig. 10 Weight changes for solid lignin residue pyrolysis at isothermal conditions of T = 523(□), 573(△), 598(☆), 623(◇), 648(○), and 673 K (×). Lines are model predictions.

Table 9 Estimated lumped kinetic parameters and heats of reactions for solid lignin residue pyrolysis

	$\text{Log}_{10}[A_i(\text{min}^{-1})]$	E_i (kJ mol^{-1})	$-\Delta H_i$ (kJ kg^{-1})
k_1	5.92 ± 0.48	74.42 ± 2.26	8780 ± 1287
k_2	6.37 ± 0.04	109.98 ± 0.06	2819 ± 871

the kinetic effects of both reaction steps on the reaction rate are more dominant. Above 573 K, a significant difference in decomposition occurs after about 35% of total weight loss. The second reaction (decomposition of polyaromatics) dominates at this stage. At a lower temperature, a longer decomposition time is required for the complete pyrolysis of lignin. The estimated kinetic parameters together with measured reaction heats for the solid lignin pyrolysis are summarized in Table 9. We can also confirm that the model gives a reasonable fit for the dynamic experimental data at the temperature ramp of 1 K min^{-1}, whose condition induces negligible thermal gradient across the sample boundary (see Fig. S2 in supplementary information†).

We also measured the heats of reactions for each reaction step. Both steps are highly exothermic and the overall heat change for lignin pyrolysis was −11 600 kJ kg^{-1}. In order to compare the thermodynamic states between lignin and pyrolysis products, we also measured the heat of combustion for the lignin using a TGA at a temperature ramp of 150 K min^{-1} under the excess oxygen environment. The combustion occurs at 673–1273 K and the heat of combustion was −33 400 kJ kg^{-1}. A comparable value (−26 700 kJ kg^{-1} for the Douglas-fir lignin combustions) can be found in the literature.[79] The heat of combustion for lignin pyrolysis is three times higher than the heat for lignin pyrolysis. This result is consistent with a product of lignin pyrolysis being carbon dioxide.

Conclusion

In this paper we have developed a lumped kinetic model of pyrolysis of Maplewood lignin based on a two step lumped

reaction mechanism. We tested two lignins extracted from Maplewood (solid lignin residue after enzymatic hydrolysis and organosolv lignin) and compared their pyrolysis behaviours with the Maplewood. The pyroprobe reactor and TGA system were used to collect intermediate products.

Lignin pyrolysis involves two series of decomposition steps. In the first step, lignin decomposed into volatiles and solid products. The solid products were primarily polyaromatics. The polyaromatics further decomposed at a temperature above 600 K. The volatile species are comprised of light gases and condensable liquid mixture. The evolution of light gaseous products was measured through Py-GC-MS and TGA-MS. CO, CO_2, and H_2O were major gaseous species. Small amounts of H_2 and CH_4 release were also observed. Condensable liquid products were captured by a nitrogen trap in a pyroprobe reactor and their concentrations were quantitatively measured as a function of pyrolysis temperature by GC-MS. The condensable liquid species were mainly composed of identifiable monomeric phenolics (14–36 carbon%) and unidentifiable heavy tars. The major detectable products were guaiacol, syringol and vanillic acid which result from the cleavage of ether linkages.

Nonvolatile solid products, polyaromatics, were collected as a solid mixture with unreacted lignin at various pyrolysis temperatures in the TGA system. Resulting solid mixtures were characterized using several analytical tools including elemental analysis, FT-IR, DP-MAS ^{13}C NMR, and TOC. Elemental analysis and TOC results showed that a larger amount of carbon transferred to the solid mixture and a larger amount of oxygen transferred to the volatile species. FT-IR and DP-MAS ^{13}C NMR analysis of the solid intermediate products indicated disappearance of methoxy groups and accumulation of nonprotonated aromatic C–C bonds with the increase in pyrolysis temperature. These results indicate that lignin pyrolysis occurs primarily from cleavage of ether bonds leaving solid polyaromatic compounds. The fraction of polyaromatics produced from lignin pyrolysis was about 0.69 which is in a good agreement with the values from pyroprobe quantification, model fitting and literature.[78]

The kinetic model was developed based on the total weight changes of nonvolatile solid mixture (unreacted lignin with polyaromatics). Constant temperature and dynamic TGA data were analyzed to estimate kinetic parameters for the two-step reaction paths of lignin pyrolysis. Lignin pyrolysis has lower activation energies and pre-exponential factors than cellulose pyrolysis. The first step in lignin pyrolysis occurs at 450–700 K with an activation energy of 74 kJ mol^{-1}. The second decomposition step has a higher activation energy (110 kJ mol^{-1}) which results in the significant accumulation of polyaromatics at a temperature above 700 K. The model developed in this study is able to predict the thermal decomposition behavior of lignin pyrolysis at isothermal conditions of a temperature range from 523 to 673 K and nonisothermal condition at 1 K min^{-1} in which no significant heat or mass transfer limitation exists. We also measured the heat of reaction for the lignin pyrolysis using DSC. The reaction steps are highly exothermic (–8780 and –2819 kJ kg^{-1} each) and thus the high exothermicity in biomass pyrolysis is attributed to the thermal contribution by the fraction of lignin content.

Acknowledgements

This material is based upon work supported by the National Science Foundation under Grant No. EFRI-0937895. This work was also supported by the Defense Advanced Research Projects Agency (DARPA) and Army Research Lab (ARL) through the Defense Science Office Cooperative Agreement W911NF-09-2-0010/09-005334 B 01 (Surf-Cat: Catalysts for production of JP-8 range molecules from lignocellulosic biomass). The views, opinions, and/or findings contained in this article are those of the authors and should not be interpreted as representing the official views or policies, either expressed or implied, of the Defense Advanced Research Projects Agency or the Department of Defense. Authors want to thank REU Student (supported by NSF) Kyle Arean-Raines. The authors thank Dr Wei Guo who helped with DP-MAS ^{13}C NMR analysis.

Notes and references

1 A. V. Bridgewater, *Thermal Science*, 2004, **8**, 21–50.
2 T. Carlson, T. Vispute and G. Huber, *ChemSusChem*, 2008, **1**, 397–400.
3 J. Diebold and J. Scahill, in *Pyrolysis Oils from Biomass*, American Chemical Society, Washington, DC, 1988, pp. 264–276.
4 R. French and S. Czernik, *Fuel Process. Technol.*, 2010, **91**, 25–32.
5 E. M. Hassan, F. Yu, L. Ingram and P. Steele, *Energy Sources, Part A*, 2009, **31**, 1829–1839.
6 G. W. Huber and A. Corma, *Angew. Chem., Int. Ed.*, 2007, **46**, 7184–7201.
7 G. W. Huber, S. Iborra and A. Corma, *Chem. Rev.*, 2006, **106**, 4044–4098.
8 P. R. Patwardhan, J. A. Satrio, R. C. Brown and B. H. Shanks, *J. Anal. Appl. Pyrolysis*, 2009, **86**, 323–330.
9 J. L. McCarthy and A. Islam, in *Lignin: Historical, Biological, and Materials Perspectives*, American Chemical Society, 1999, vol. 742, ch. 1, pp. 2–99.
10 T. Nimmanwudipong, R. Runnebaum, D. Block and B. Gates, *Catal. Lett.*, 2011, **141**, 779–783.
11 J. Zakzeski, P. C. A. Bruijnincx, A. L. Jongerius and B. M. Weckhuysen, *Chem. Rev.*, 2010, **110**, 3552–3599.
12 F. S. Chakar and A. J. Ragauskas, *Ind. Crops Prod.*, 2004, **20**, 131–141.
13 D. V. Evtuguin, C. Pascoal Neto, J. Rocha and J. D. Pedrosa de Jesus, *Appl. Catal., A*, 1998, **167**, 123–139.
14 E. Dorrestijn, L. J. J. Laarhoven, I. W. C. E. Arends and P. Mulder, *J. Anal. Appl. Pyrolysis*, 2000, **54**, 153–192.
15 D. Fengel and G. Wegener, *Wood: Chemistry, Ultrastructure, Reactions*, Walter de Gruyter Inc, Berlin, 1989.
16 G. Jiang, D. J. Nowakowski and A. V. Bridgwater, *Thermochim. Acta*, 2010, **498**, 61–66.
17 X. Pan, N. Gilkes, J. Kadla, K. Pye, S. Saka, D. Gregg, K. Ehara, D. Xie, D. Lam and J. Saddler, *Biotechnol. Bioeng.*, 2006, **94**, 851–861.
18 T. N. Kleinert, US Patent 3,585,104, 1971.
19 F. Pla, M. Dolk, J. F. Yan and J. L. McCarthy, *Macromolecules*, 1986, **19**, 1471–1477.
20 E. A. Capanema, M. Y. Balakshin and J. F. Kadla, *J. Agric. Food Chem.*, 2005, **53**, 9639–9649.
21 C. Sievers, M. B. Valenzuela-Olarte, T. Marzialetti, I. Musin, P. K. Agrawal and C. W. Jones, *Ind. Eng. Chem. Res.*, 2009, **48**, 1277–1286.
22 C. Wyman, *Handbook on Bioethanol: Production and Utilization*, Taylor & Francis, Washington, DC, 1996.
23 J. Jae, G. A. Tompsett, Y.-C. Lin, T. R. Carlson, J. Shen, T. Zhang, B. Yang, C. E. Wyman, W. C. Conner and G. W. Huber, *Energy Environ. Sci.*, 2010, **3**, 358–365.
24 F. J. Kilzer and A. Broido, *Pyrodynamics*, 1965, **2**, 151–163.
25 A. Broido, ed. F. Shafizadeh, K. V. Sarkanen and D. A. Tillman, Academic, New York, 1976, pp. 19–36.
26 A. G. W. Bradbury, Y. Sakai and F. Shafizadeh, *J. Appl. Polym. Sci.*, 1979, **23**, 3271–3280.
27 R. K. Agrawal, *Can. J. Chem. Eng.*, 1988, **66**, 403–412.

28 D. G. Radlein, J. Piskorz and D. S. Scott, *J. Anal. Appl. Pyrolysis*, 1991, **19**, 41–63.
29 G. Várhegyi, E. Jakab and M. J. Antal, *Energy Fuels*, 1994, **8**, 1345–1352.
30 J. P. Diebold, *Biomass Bioenergy*, 1994, **7**, 75–85.
31 J. L. Banyasz, S. Li, J. Lyons-Hart and K. H. Shafer, *J. Anal. Appl. Pyrolysis*, 2001, **57**, 223–248.
32 V. Mamleev, S. Bourbigot and J. Yvon, *J. Anal. Appl. Pyrolysis*, 2007, **80**, 141–150.
33 Y.-C. Lin, J. Cho, G. A. Tompsett, P. R. Westmoreland and G. W. Huber, *J. Phys. Chem. C*, 2009, **113**, 20097–20107.
34 J. Cho, J. M. Davis and G. W. Huber, *ChemSusChem*, 2010, **3**, 1162–1165.
35 A. E. Lipska and Frank A. Wodley, *J. Appl. Polym. Sci.*, 1969, **13**, 851–865.
36 T. Hirata, *Ringyo Shikenjo Kenkyu Hokoku*, 1974, **263**, 1–16.
37 I. Milosavlevic and E. Suuberg, *Ind. Eng. Chem. Res.*, 1995, **34**, 1081–1091.
38 P. Aggarwal, D. Dollimore and K. Heon, *J. Therm. Anal.*, 1997, **50**, 7–17.
39 M. J. Antal, G. Várhegyi and E. Jakab, *Ind. Eng. Chem. Res.*, 1998, **37**, 1267–1275.
40 M. Grønli, M. J. Antal, Jr. and G. Varhegyi, *Ind. Eng. Chem. Res.*, 1999, **38**, 2238–2244.
41 H. Yang, R. Yan, H. Chen, D. H. Lee and C. Zheng, *Fuel*, 2007, **86**, 1781–1788.
42 A. Beste and A. C. Buchanan, *J. Org. Chem.*, 2009, **74**, 2837–2841.
43 J.-Y. Liu, S.-B. Wu and R. Lou, *BioResources*, 2011, **6**, 1079–1093.
44 J. A. Caballero, R. Font and A. Marcilla, *J. Anal. Appl. Pyrolysis*, 1996, **36**, 159–178.
45 J. A. Caballero, R. Font and A. Marcilla, *J. Anal. Appl. Pyrolysis*, 1996, **38**, 131–152.
46 H. E. Jegers and M. T. Klein, *Ind. Eng. Chem. Process Des. Dev.*, 1985, **24**, 173–183.
47 P. Murugan, N. Mahinpey, K. E. Johnson and M. Wilson, *Energy Fuels*, 2008, **22**, 2720–2724.
48 E. Ranzi, A. Cuoci, T. Faravelli, A. Frassoldati, G. Migliavacca, S. Pierucci and S. Sommariva, *Energy Fuels*, 2008, **22**, 4292–4300.
49 H. H. King, P. R. Solomon, E. Avni and R. W. Coughlin, *Preprint Papers - American Chemical Society, Division of Fuel Chemistry*, 1983, **28**, 319–329.
50 R. S. Miller and J. Bellan, *Combust. Sci. Technol.*, 1997, **126**, 97–137.
51 E. Avni and R. W. Coughlin, *Thermochim. Acta*, 1985, **90**, 157–167.
52 D. Ferdous, A. K. Dalai, S. K. Bej and R. W. Thring, *Energy Fuels*, 2002, **16**, 1405–1412.
53 G. Várhegyi, M. J. Antal, E. Jakab and P. Szabó, *J. Anal. Appl. Pyrolysis*, 1997, **42**, 73–87.
54 Q. Liu, S. Wang, Y. Zheng, Z. Luo and K. Cen, *J. Anal. Appl. Pyrolysis*, 2008, **82**, 170–177.
55 T. R. Nunn, J. B. Howard, J. P. Longwell and W. A. Peters, *Ind. Eng. Chem. Process Des. Dev.*, 1985, **24**, 844–852.
56 B. Iatridis and G. R. Gavalas, *Ind. Eng. Chem. Prod. Res. Dev.*, 1979, **18**, 127–130.
57 E. Avni, R. W. Coughlin, P. R. Solomon and H. H. King, *Preprint Papers - American Chemical Society, Division of Fuel Chemistry*, 1983, **28**, 307–318.
58 E. Avni, R. W. Coughlin, P. R. Solomon and H. H. King, *Fuel*, 1985, **64**, 1495–1501.
59 H. E. Kissinger, *Anal. Chem.*, 1957, **29**, 1702–1706.
60 J. A. Conesa, A. Marcilla, J. A. Caballero and R. Font, *J. Anal. Appl. Pyrolysis*, 2001, **58–59**, 617–633.
61 G. Jiang, D. J. Nowakowski and A. V. Bridgwater, *Energy Fuels*, 2010, **24**, 4470–4475.
62 E. A. Capanema, M. Y. Balakshin and J. F. Kadla, *J. Agric. Food Chem.*, 2004, **52**, 1850–1860.
63 K. M. Holtman, N. Chen, M. A. Chappell, J. F. Kadla, L. Xu and J. Mao, *J. Agric. Food Chem.*, 2010, **58**, 9882–9892.
64 R. Bayerbach and D. Meier, *J. Anal. Appl. Pyrolysis*, 2009, **85**, 98–107.
65 V. Cozzani, A. Lucchesi, G. Stoppato and G. Maschio, *Can. J. Chem. Eng.*, 1997, **75**, 127–133.
66 M. J. Antal and M. Grønli, *Ind. Eng. Chem. Res.*, 2003, **42**, 1619–1640.
67 N. Y. Chen, T. F. D. Jr. and L. R. Koenig, *Chemtech.*, 1986, **16**, 506–511.
68 T. P. Vispute, H. Zhang, A. Sanna, R. Xiao and G. W. Huber, *Science*, 2010, **330**, 1222–1227.
69 H. Zhang, Y.-T. Cheng, T. P. Vispute, R. Xiao and G. W. Huber, *Energy Environ. Sci.*, 2011, **4**, 2297–2307.
70 C. E. L. Pasquali and H. Herrera, *Thermochim. Acta*, 1997, **293**, 39–46.
71 R. K. Sharma, J. B. Wooten, V. L. Baliga, X. Lin, W. Geoffrey Chan and M. R. Hajaligol, *Fuel*, 2004, **83**, 1469–1482.
72 N. Wang and M. J. D. Low, *Mater. Chem. Phys.*, 1990, **26**, 67–80.
73 P. F. Britt, A. C. Buchanan, M. J. Cooney and D. R. Martineau, *J. Org. Chem.*, 2000, **65**, 1376–1389.
74 H. Ben and A. J. Ragauskas, *Energy Fuels*, 2011, **25**, 2322–2332.
75 Y.-R. Luo, *Comprehensive Handbook of Chemical Bond Energies*, Taylor and Francis Group, Boca Raton, 2007.
76 H. Kawamoto, M. Ryoritani and S. Saka, *J. Anal. Appl. Pyrolysis*, 2008, **81**, 88–94.
77 R. Narayan and M. J. Antal, *Ind. Eng. Chem. Res.*, 1996, **35**, 1711–1721.
78 M. J. Antal, *Ind. Eng. Chem. Prod. Res. Dev.*, 1983, **22**, 366–375.
79 R. M. Rowell, ed., *Handbook of Wood Chemistry and Wood Composites*, CRC Press, Boca Raton, 2005.